Thermal and Fluid Flow Analysis of Shell-and-Tube Heat Exchangers with Smooth and Dimpled Tubes

Ibrahim A. FETUGA[1,*], *Olabode T. OLAKOYEJO*[1], *Adeola S. SHOTE*[2], *Gbeminiyi M. SOBAMOWO*[1], *Omotayo OLUWATUSIN*[1], *Joshua K. GBEGUDU*[1]

[1]Department of Mechanical Engineering, University of Lagos, Akoka, Yaba, Lagos, Nigeria
[2]Department of Mechanical Engineering, Olabisi Onabanjo University, Ago-Iwoye, Nigeria

*Corresponding Author: Ibrahim A. FETUGA (Email: fetugaebraheem@gmail.com)
(Received: 6-Apr-2022; accepted: 1-Aug-2022; published: 30-Sep-2022)
DOI: http://dx.doi.org/10.55579/jaec.202263.378

Abstract. *This current work mainly focuses on the enhancement of the heat transfer and fluid flow characteristics of shell-and-tube heat exchangers by incorporating dimples on the smooth or conventional tubes. With the aid of the ANSYS (Fluent) commercial software package, Computational Fluid Dynamics (CFD) simulations under a steady-state condition were conducted on heat exchanger having a single shell and 12 tubes (with or without dimples), 50% baffle cut, 100mm baffle spacing and turbulent flow. The temperature, velocity, and pressure fields at the shell and tube zone in both cases are analyzed. The computational fluid dynamics results of the heat exchanger with dimpled tubes are compared with conventional (smooth) tubes. However, the results show that a shell and tube heat exchanger with dimpled tubes has a higher overall heat transfer coefficient than that of conventional (smooth) tubes.*

Keywords

Shell-and-Tube heat exchanger, Heat transfer coefficient, Smooth, Dimples, Realizable k-epsilon.

1. Introduction

Heat exchangers are thermal devices designed to allow the exchange of heat between two fluids. The fluid may be multiphase or single phase, determined by the purpose the heat exchanger is being used for. Heat exchangers find their applications in both domestic and commercial purposes, such as nuclear plants, power plants, heating, ventilation, and air conditioning (HVAC), and food processing plants [1]–[5]. Heat exchangers come in a variety of shapes and sizes, but the most common types are shell-and-tube, plate-and-frame, and scraped surface heat exchangers [6]–[8]. Shell and tube heat exchanger (STHE) contains a shell and a bundle of tubes, where one fluid medium flows through the shell and the other runs via the tube bundle [9, 10]. Augmentation of the thermal performance of SHTE depends on numerous factors, which include flow configuration (parallel, counter, and cross-flow), geometry configuration of the shell, tube layout pattern, tube shape, tube configuration (plain, corrugated, longitudinal finned, dimple and protrusion), number of baffles, baffle cut, type, shape, and spacing [11]–[15].

Several studies on the enhancement of the thermal performance of STHEs have been worked on by researchers and published in the

literature. Vignesh et al. [16] explored the influence of spherical dimples on the thermal characteristics of the heat exchanger through both computational and experimental approaches. From their CFD results, it was reported that the dimpled tube has a greater temperature rise and pressure drop than the smooth tube. Meanwhile, from their experimental results, it was found that when a dimpled tube is used instead of a smooth tube, the overall heat transfer coefficient improves by 54 percent to 56 percent. Serrao et al. [17] used ANSYS (Fluent) to perform a comparative study on the smooth tube and corrugated tube. They suggested that the corrugated tube had a 54.7% increase in overall heat transfer coefficient when compared to the smooth tube. Xie et al. [18] numerically studied the improvement of heat transfer rate and hydrodynamic structure in an ellipsoidal dimpled tube. They asserted that a dimpled tube improves the thermal performance of STHE. Banekar et al. [19] suggested that thermal performance is improved in a dimpled tube when compared to other tube geometrical configurations. Matos et al. [20] conducted an optimization study for heat transfer enhancement under force convection for both elliptic tubes and staggered finned circular tube at Reynolds number ranging from 300 to 800. It was concluded that elliptical tube has about a 20% increase in heat transfer as compared to the staggered circular tube. Jozaei et al. [21] investigated the impact of the space or distance between the baffles on the thermal and hydrodynamic performance of heat exchangers. It was reported that shorter baffle spacing increased the heat transfer coefficient and pressure drop. Li et al. [22] numerically investigated the heat transfer coefficient and pressure drop in elliptical and circular pipes at a constant wall temperature. The results indicated that the elliptical tube showed better thermal performance and a 30%-40% increase in pressure drop than that of circular tubes. Shahdad et al. [23] carried out studies on the heat transfer rate of plain and perforated plate-fin heat exchangers. It was revealed that perforated plate-fin has a higher heat transfer coefficient and Nusselt number than plain fin. Sridharan et al. [24] investigated the accuracy of the fuzzy logic expert systems (Sugeno and Mamdani) in predicting the outlet temperature of a double-pipe heat exchanger. He compared the results obtained from the respective fuzzy logic with the outcomes from the experiment he conducted at a mass flow rate ranging from 1 to 4kg/min. According to his findings, he indicated that the results of the Sugeno-based predictive values are satisfactory with the experimental data as compared to the Mamdani-based predictive values.

Many attempts to enhance the performance of shell-and-tube heat exchangers by considering various factors such as the baffle plates and shell side layout have been made by previous researchers, with little attention paid to the tube side of the heat exchangers. Therefore, this novel design of the shell and tube heat exchanger with dimpled tubes is proposed to increase the performance of the conventional heat exchanger. In this study, ANSYS commercial software codes were adopted to conduct a three-dimensional numerical simulation on both conventional STHE and proposed STHE. The temperature, pressure, velocity field, and overall heat transfer coefficient at the shell and tube side of the dimpled STHE are investigated and compared with the conventional shell and tube heat exchanger. The benefits of this proposed STHE are not only restricted to students and future researchers but also extended to industries as a waste heat recovery system for pre-heating purposes.

2. Methodology

2.1. Geometry Description

ANSYS Design Modeler was used to design the three-dimensional geometry of STHE. In this study, we considered two different cases of shell-and-tube heat exchangers. The first case is a STHE having a single shell and a bundle of smooth tubes, whereas the second case is the STHE with a single shell and bundle of dimpled tubes, as shown in Figs. 1 and 2. The details of the geometry parameters for the two cases investigated are given in Tab. 1. The parameters for the dimple are given in Tab. 2. The various boundary conditions (inlets and outlets) used in the CFD software for this study are shown in Tab. 3.

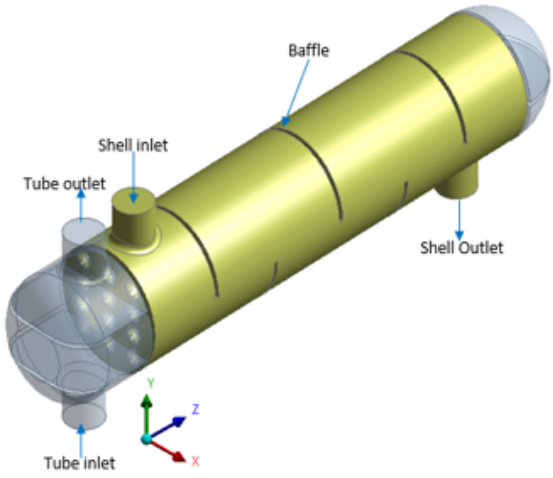

Fig. 1: Schematic representation of STHE.

Tab. 1: Geometry parameters.

Part	Parameter	Smooth tube	Dimpled tubes
	Length of heat Exchanger	815 mm	815 m
Shell	Shell diameter (S_D)	150 mm	150 mm
	Shell length (S_L)	600 mm	600 mm
	Shell material	Steel	Steel
Tube	Tube diameter (t_D)	20 mm	20 mm
	Tube length (t_L)	620 mm	620 mm
	Number of tubes (N_t)	12	12
	Tube material	Steel	Steel
Baffle	Number of baffles (N_B)	5	5
	Baffle cut (B_c)	50%	50%
	Baffle spacing (B_s)	100 mm	100 mm
	Baffle thickness (B_t)	5 mm	5 mm

Tab. 2: Details of the Dimple Configuration.

Radius	3 mm
Depth	1.5 mm
Shape	spherical
Dimple spacing	17.5 mm
Number of spheres	175

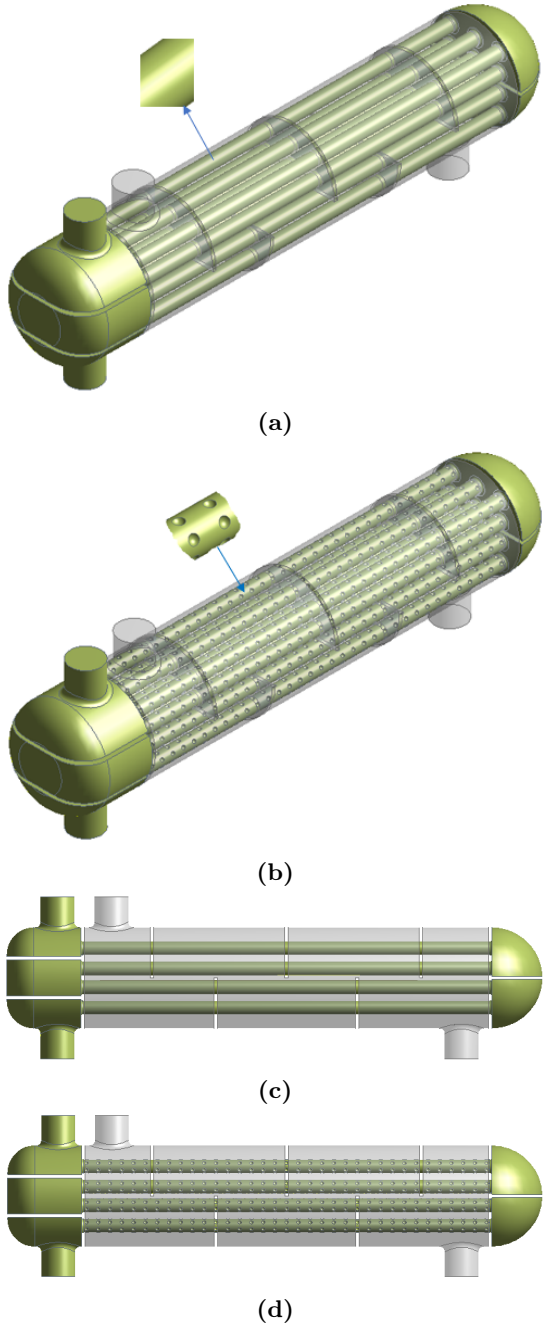

Fig. 2: (a) 3D view of STHE with plain/smooth tubes (b) 3D view of STHE with dimpled tubes (c) 2D view of the STHE with smooth/plain tubes (d) 2D view of the STHE with dimpled tubes.

2.2. Mesh Generation

The size and shape of the grid must be taken into consideration when aiming at the accuracy of the computations. ANSYS Mesh was employed to generate unstructured tetrahedral grids with a size of 0.0001 for both the shell and the tubes. The generated grid in Fig. 3 was about 1.1 million.

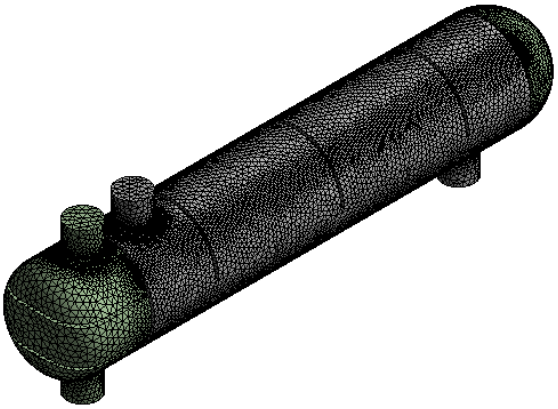

Fig. 3: Unstructured tetrahedral mesh for the computational domain.

2.3. Problem Formulation

The governing equations, assumptions, and boundary conditions employed in this investigation are explained in this section. The problem is solved by employing Reynolds averaged Navier-Stokes equations [25]–[27] in the ANSYS software. Equations for energy, momentum, and continuity [25]–[27] are solved iteratively until convergence is attained. The governing equations are presented in Eqs. (1)-(7). The governing equations are simplified much further with the following assumptions:

(i) Steady-state, turbulent, 3D incompressible flow and heat transfer;

(ii) Single-phase fluid;

(iii) The thermo-physical properties of the fluids and solid are constant;

(iv) Thermal radiation and magnetic force are ignored.

The boundary conditions used for the computations are in Tab. 3.

Continuity equation

$$\nabla \cdot (\rho V) = 0 \tag{1}$$

Momentum equation
x-direction;

$$\nabla \cdot (\rho u V) = -\frac{\delta \rho}{\delta x} + \left(\frac{\delta \tau_{xx}}{\delta x} + \frac{\delta \tau_{yx}}{\delta y} + \frac{\delta \tau_{zx}}{\delta z}\right) \tag{2}$$

y-direction;

$$\nabla \cdot (\rho v V) = -\frac{\delta \rho}{\delta y} + \left(\frac{\delta \tau_{xy}}{\delta x} + \frac{\delta \tau_{yy}}{\delta y} + \frac{\delta \tau_{zy}}{\delta z}\right) + \rho g \tag{3}$$

z-direction;

$$\nabla \cdot (\rho w V) = -\frac{\delta \rho}{\delta z} + \left(\frac{\delta \tau_{xz}}{\delta x} + \frac{\delta \tau_{yz}}{\delta y} + \frac{\delta \tau_{zz}}{\delta z}\right) \tag{4}$$

Energy equation

$$\nabla \cdot (\rho e V) = -\rho \nabla \cdot V + \nabla \cdot (k \nabla T) + q + \varphi \tag{5}$$

For heat dissipation φ;

$$\begin{aligned} \varphi = \mu \Bigg[2\Big[\Big(\frac{\delta u}{\delta x}\Big)^2 + \Big(\frac{\delta v}{\delta y}\Big)^2 + \Big(\frac{\delta w}{\delta z}\Big)^2\Big] \\ + \Big[\Big(\frac{\delta u}{\delta y} + \frac{\delta v}{\delta x}\Big)^2 + \Big(\frac{\delta u}{\delta z} + \frac{\delta v}{\delta x}\Big)^2 + \Big(\frac{\delta v}{\delta z} + \frac{\delta w}{\delta y}\Big)^2\Big] \Bigg] \\ + \lambda (\nabla \cdot V)^2 \end{aligned} \tag{6}$$

Turbulence modeling
The $k - \varepsilon$ realizable turbulence equation is expressed below with its coefficient and closure functions [27, 28].

$$\begin{aligned} \frac{\delta}{\delta x_j}(\rho \varepsilon u_j) = \frac{\delta}{\delta x_j}\left(\left(\mu + \frac{\mu_t}{\sigma_\varepsilon}\right)\frac{\delta \varepsilon}{\delta x_j}\right) + \rho C_1 S \varepsilon \\ + C_{1\varepsilon}\frac{\varepsilon}{k} C_{2\varepsilon} G_b - C_2 \rho \frac{\varepsilon^2}{k + \sqrt{\varepsilon v}} + S_v \end{aligned} \tag{7}$$

where $C_{1\varepsilon} = 1.43$, $C_{2\varepsilon} = 1.91$, $\sigma_k = 1$, and $\sigma_\varepsilon = 1.25$.

The temperature change ΔT_1, between the hot water in the shell inlet and the hot water in the tube outlet was estimated as [29, 30]:

$$\Delta T_1 = T_{si} - T_{to} \tag{8}$$

Tab. 3: Boundary Conditions.

Shell side	
Inlet temperature of hot water (T_{si})	$65°C$
Mass flow rate ($\dot{m}_{hw}$)	0.5 kg/s
Shell outlet (P_{so})	Guage pressure equals 0 Pa
Shell wall	adiabatic, No-slip condition, and Stationary
Tube side	
Inlet temperature of cold water (T_{ti})	$10°C$
Mass flow rate ($\dot{m}_{cw}$)	0.2 kg/s
Tube outlet (P_{to})	Guage pressure equals to 0 Pa
Shell/Tubes interface	
Coupled	
Thermal properties of water at mean temperature ($37.5°C$)	
Thermal conductivity (k)	$0.6 Wm^{-1}K^{-1}$
Specific heat capacity (cp)	Hot water: 4186.5 $Jkg^{-1}K^{-1}$, Cold water: 4180 $Jkg^{-1}K^{-1}$
Dynamic viscosity (μ)	0.001003 $Kgm^{-1}s^{-1}$
Density (ρ)	998 kgm^{-3}
Thermal properties of solid material (Steel)	
Thermal conductivity (k_s)	16.27 $Wm^{-1}K^{-1}$
Specific heat capacity (c_{ps})	502.48 $Jkg^{-1}K^{-1}$
Density (ρ_s)	8030 kgm^{-3}

The temperature change ΔT_2, between the cold water at the shell outlet and the cold-water at the tube inlet was expressed as [29, 30]:

$$\Delta T_2 = T_{so} - T_{ti} \tag{9}$$

The mean fluid temperature ΔT_m, which is the average of temperature change ΔT_1 and temperature change ΔT_2 was expressed as [29, 30]:

$$\Delta T_m = \frac{\Delta T_1 + \Delta T_2}{2} \tag{10}$$

The logarithmic temperature difference between the temperature change ΔT_1 and ΔT_2 was defined as [29, 30]:

$$\Delta T_{lm} = \frac{\Delta T_1 - \Delta T_2}{ln\left(\frac{\Delta T_1}{\Delta T_2}\right)} \tag{11}$$

The heat transfer rate $\dot{Q}_{sh}$ from the hot water in the shell was defined as [30]–[32]:

$$\dot{Q}_{sh} = \dot{m}_s C_{p,s}(T_{si} - T_{to}) = U A_s \Delta T_{lm} \tag{12}$$

where U represents the overall heat transfer coefficient, $C_{p,s}$ denotes the specific heat capacity of the hot water, which is estimated at the mean fluid temperature and $\dot{m}_s$ is the mass flow rate of the hot water flowing in the shell. Thus, the overall heat transfer coefficient U is defined as [30]:

$$U = \frac{\dot{m}_s(T_{si} - T_{to})}{A_s \Delta T_{lm}} \tag{13}$$

2.4. Computation Procedures

ANSYS (Fluent) software code was used to solve the continuity, momentum, and energy equations aforementioned in problem formulation. The simulation was performed on an ASUS Intel Core i5-7200U CPU with a processor speed up to 3.5GHz with 16GB of memory, under the parallel version with double precision operating condition of ANSYS software. A pressure-based solver and a realizable $k - \varepsilon$ turbulence model were chosen for this computation. The SIMPLE algorithm was selected for pressure-velocity coupling, and a second-order upwind scheme was used for both pressure and momentum. Under-relaxation factors were left as default values, and all equations were set at convergence criteria of 1×10^{-7}. Each run takes about 20hours to converge.

Grid independence was checked by increasing the grid significantly till no change was observed in the enthalpy balance in the shell-side.

3. Results and Discussion

3.1. Grid Independence Test

The grid independence test is conducted for the case of smooth tubes to ensure efficient computation resources through the selection of an appropriate number of grids. Table 4 reveals the influence of the number of grids on the inlet and outlet mass flow rate and enthalpy. As shown in Tab. 4, all grids show a negligible error in mass balance, while in enthalpy balance, the grid (1142016) has a reasonable computation time and insignificant error as compared to

Tab. 4: Grid Independence test.

No. of grids	No. of iterations	Computation time (hrs.)	Shell side					
			Mass balance (kg/s)			Enthalpy balance (W)		
			Inlet	Outlet	Error (%)	Inlet	Outlet	Error (%)
661039	1211	8	0.5	0.5	0	26921	26679	0.9
1142016	2771	18	0.4	0.4	0	24193	24072	0.5
1912750	3217	22	0.3	0.3	0	22852	22395	2

others. Therefore, a grid (1142016) was chosen for the computation.

3.2. Model Validation

In this section, the model is validated by conducting simulations for a smooth and a dimpled tube at a mass flow rate ranging from 0.2kg/s to 0.5kg/s with a corresponding Reynolds number of 12689 to 31772. The boundary conditions and geometric parameters of the smooth tube and dimple tube used for the validation remained unchanged with those adopted for this study. The results (Nusselt number and friction factor) obtained from the numerical simulations for the smooth and dimpled tube are compared with Wang et al. correlation [33]. As can be seen in Fig. 4, the minimum and maximum deviation in the Nusselt number between the simulation results and Wang et al. [33] for the smooth tube are -10% and 6%, respectively. Whereas a minimum and maximum deviation of -7% and 4% are reported in the case of dimpled tube when compared with the correlation proposed by Wang et al. [33] Fig. 5 presents the comparison of the friction factor between the simulation results and the available correlation. It is revealed in Fig. 5 that the minimum and maximum deviation between the simulation data obtained for the smooth tube and the Wang et al. correlation [33] is -9% and 6%. Meanwhile, the minimum and maximum deviation error between the dimpled tube and that of Wang et al. [33] correlation is -5% and 3%, respectively. Thus, it can be concluded that the simulation data obtained in this research has a substantial validity as a result of insignificant difference between the simulation results and available correlations. However, this has raised our confidence in this research.

Heat transfer correlation for the smooth and dimpled tube are expressed in Eq. (14) and Eq. (15) below;

Wang et al. [33] correlation for smooth tube

$$Nu_s = 0.0184Re^{0.768} \tag{14}$$

Wang et al. [33] correlation for dimpled tube

$$Nu_t = 0.098Re^{0.655}Pr^{\frac{1}{3}} \tag{15}$$

where Nu, Re, f, and Pr denotes the Nusselt number, Reynolds number and Prandtl number, respectively.

Friction factor (f) for the smooth and dimpled tube is predicted by using a correlation proposed by Wang et al. [33] in Eq. (16) and Eq. (17), respectively.

Wang et al. [33] correlation for smooth tube

$$f = (1.82log - 1.64)^{-2} \tag{16}$$

Wang et al. [33] correlation for dimpled tube

$$f = 0.432Re^{-0.221} \tag{17}$$

3.3. CFD Result and Comparison of the Performance of STHE with Smooth Tubes and Dimpled Tubes

Table 5 shows the results for STHE with smooth tubes and dimpled tubes. The boundary conditions and configurations of tubes and shell are all the same for both cases. As presented in Tab. 5, in the shell zone, the cooling and pressure of the hot water decreased for both cases.

Tab. 5: CFD results for the STHE with smooth tubes and dimpled tubes.

	Parameter	Smooth tubes (conventional)	Dimpled tubes (Modified)	Remarks
Shell side	Inlet temp($°C$)	65	65	-
	Outlet temp ($°C$)	61.6	61.2	Cooling of the hot water increased
	Temp drop (ΔT)	**3.4**	**3.8**	
	Inlet pressure (Pa)	65.86	54.602	
	Outlet pressure (Pa)	0	0	Pressure of the hot water decreased
	Pressure drop (ΔP)	**65.86**	**54.60**	
Tube side	Inlet temp($°C$)	10	10	
	Outlet temp ($°C$)	20.6	22.2	Heating of the cold water increased
	Temp rise (ΔT)	**10.6**	**12.2**	
	Inlet pressure (Pa)	166.7	203.4	
	Outlet pressure (Pa)	0	0	Pressure of the cold water reduced
	Pressure drop (ΔP)	**166.7**	**203.4**	
	Overall heat transfer coefficient (W/m^2K)	1060.41	1210.6	Overall heat transfer coefficient increased

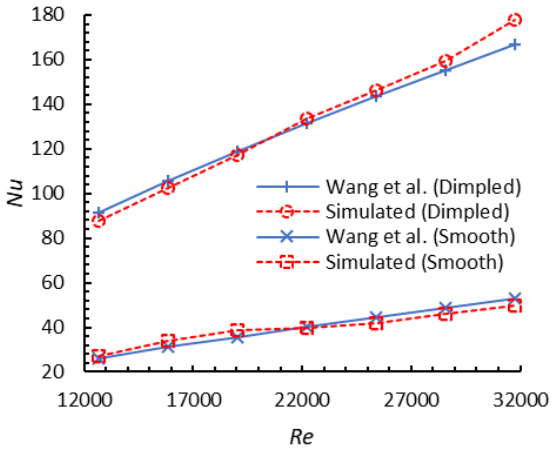

Fig. 4: Nu vs Re for smooth tube and dimpled tube.

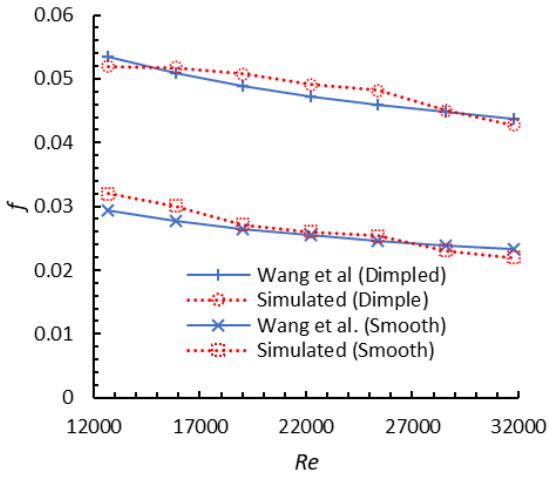

Fig. 5: f vs Re for smooth tube and dimpled tube.

The STHE with dimpled tubes has a higher temperature drop and pressure drop. The pressure and temperature increased by 10.5% and 18.7%, respectively, as compared to the heat exchanger having smooth tubes. This increases the temperature at the wall surface and hence increases the temperature difference between the fluid and the wall. Similarly, in the tube zone, the heating of the cold water increased and the pressure of the cold water reduced. Temperature change and pressure drop were seen to be higher in the case of dimpled tubes as compared to smooth tubes. The temperature change and pressure drop increased by 15% and 22%, respectively, for the case of STHE with the dimpled tubes as compared with smootCFD result and comparison of the performance of STHE with smooth tubes and dimpled tubes. The reason for increased temperature in dimpled STHE is that turbulence is generated by the dimples. These dimples cause disruption to the flow and then facilitate the mixing of the fluid, while the augmentation in the pressure drop is a result of the frictional forces exerted on the flow by the dimples in the tube-side coupled with the constriction in the flow area. However, the overall heat transfer coefficient for the case of dimpled

tubes is 14% more than that of smooth tubes. The increase in overall heat transfer coefficient in STHE with dimpled tubes is as a result of the turbulence generated by the dimples.

3.4. Temperature distribution

Figures 6 and 7 show the variation of maximum temperature along the z-axis at various sections of the STHE in the shell-side and tube-side for the case of conventional and dimpled tubes. A similar trend of temperature degradation is observed in the shell and tube side for both conventional and dimpled tubes. The only noticeable difference is that maximum temperature difference in the shell-side between the conventional STHE and STHE with dimpled tubes is relatively appreciable as compared to that of the tube-side. Furthermore, for the shell side, there is no significant difference in maximum temperature between the two proposed designs at $z = 50$ mm. For the tube side, reverse is the case of tube side at $z = 50$ mm, whereas negligible difference in maximum temperature is observed at $z = 550$ mm. Figures 8 and 9 visualize the temperature contour along the x-y plane at various sections of the z-axis of the heat exchanger in the shell-side and tube-side, respectively. Figure 8 reveals that the temperature of the hot water in the shell zone gradually declines from the inlet (left) to the outlet (right), whereas the temperature of the cold water in the tube zone (see Fig. 9) increases from the inlet (down) to the outlet (up). This shows that heat is being dissipated by the hot water flowing across the shell as cold water subsequently flows from the inlet to the outlet of the tube. In the shell zone (see Figs. 8a and 8b), at axial location ($z = 50$ mm, which is proximal to the inlet of the shell side), the same magnitude of mass flow temperature ($64.4°C$) is observed in both STHEs. Meanwhile, at axial location ($z = 550$ mm, which is distal to the inlet of the shell side), the maximum mass flow temperature of $59°C$ and $58.2°C$ is reported in conventional STHE and STHE with dimpled tubes, respectively. In the tube zone (see Figs. 9a and 9b), at axial location ($z = 50$ mm, which is close to the outlet of the tube-side), the maximum mass flow temperature in the STHE with dimpled tubes is relatively higher than that of conventional STHE by $2.3°C$. Figure 10 depicts the temperature contour along the y-z plane at the mid-section of the STHE.

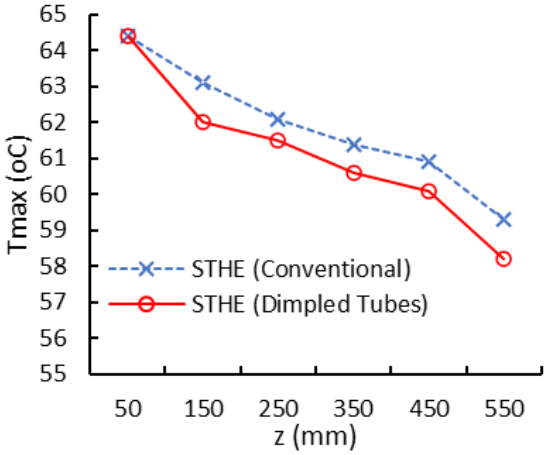

Fig. 6: Tmax ($°C$) along x-y plane vs z (mm) in the shell-side.

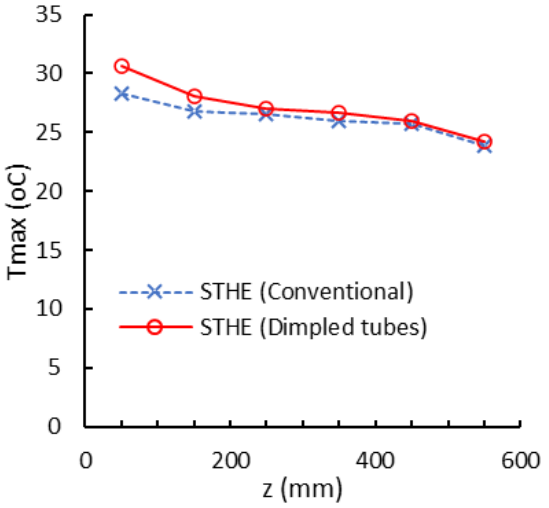

Fig. 7: Tmax ($°C$) along x-y plane vs z (mm) in the tube-side.

3.5. Pressure contour

Figure 11 presents the pressure variation along the y-z plane at the mid-section (x-axis) of the heat exchanger. Pressure drop is evident from the inlet to the outlet at the both shell and tube-side. More so, the pressure drop in the shell

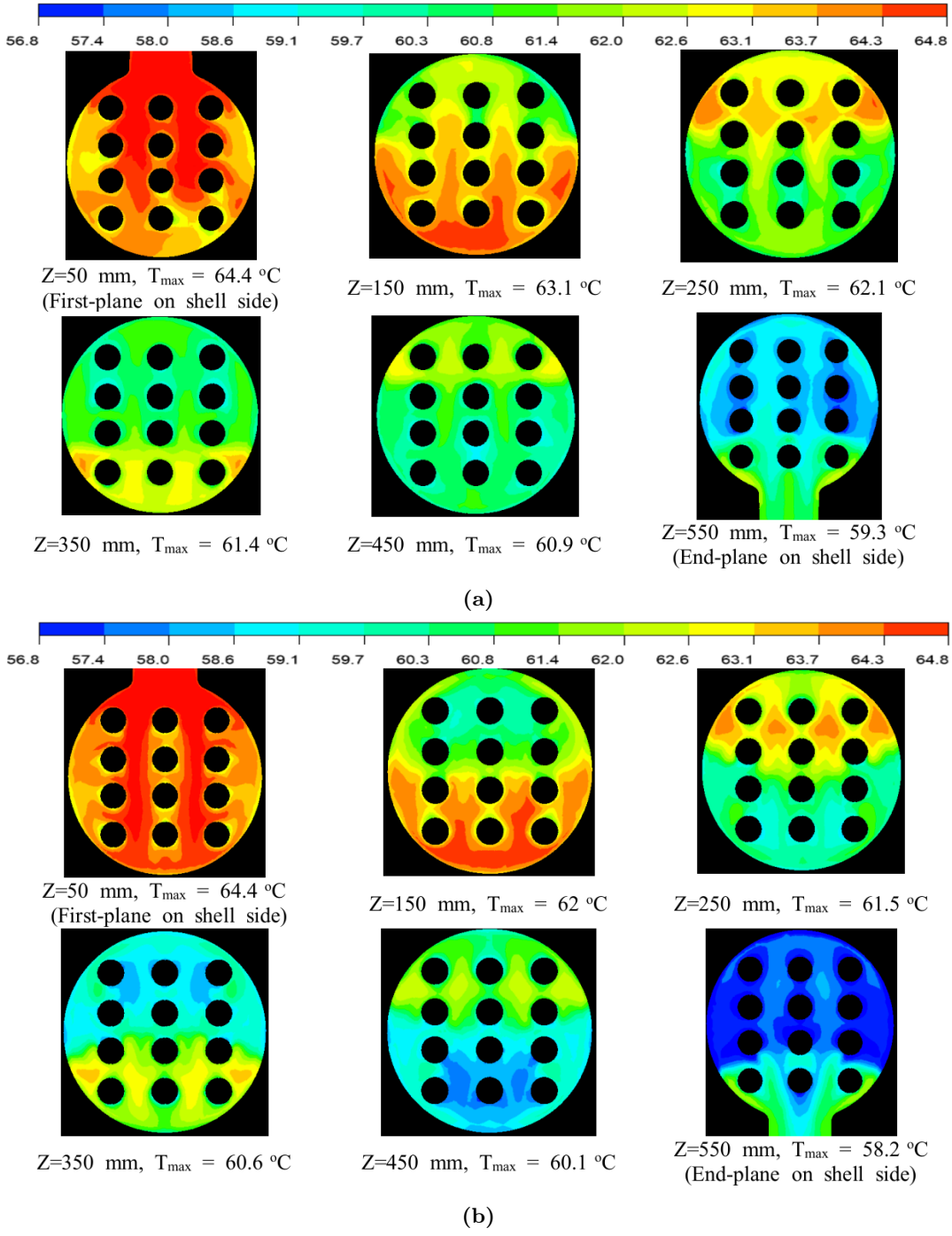

Fig. 8: (a) Temperature ($^{\circ}C$) distribution along x-y section plane at various axial locations (z-axis) in shell-side for STHE with smooth tubes (conventional). (b) Temperature ($^{\circ}C$) distribution along x-y section plane at various axial locations (z-axis) in shell-side for STHE with dimpled tubes (modified).

side of the conventional STHE is gradually decreasing as compared to the pressure drop in the STHE with dimpled tubes. whereas pressure declines uniformly from the tube inlet to the exit

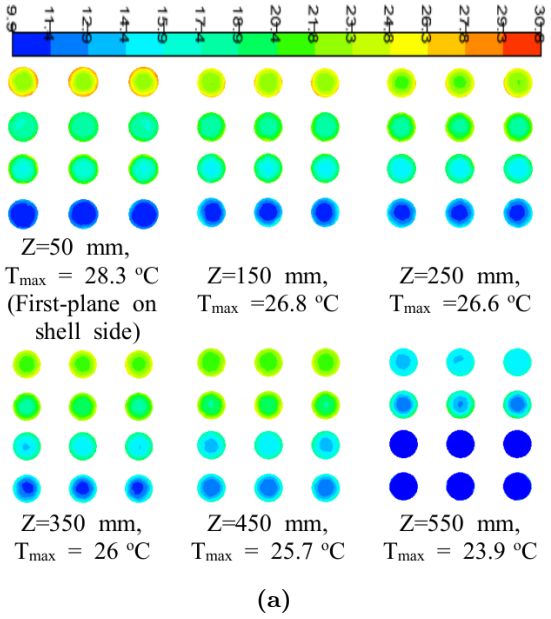

Fig. 9: (a) Temperature ($°C$) distribution along x-y section plane at various axial locations (z-axis) in tube-side for STHE with smooth tubes (conventional). (b) Temperature ($°C$) distribution along x-y section plane at various axial locations (z-axis) in tube-side for STHE with dimpled tubes (modified).

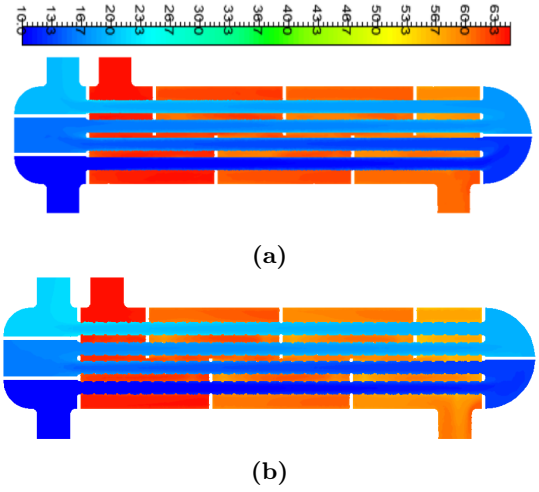

Fig. 10: Temperature ($°C$) distribution along y-z section plane at the mid-section of heat exchanger for (a) STHE with smooth tubes (b) STHE with dimpled tubes.

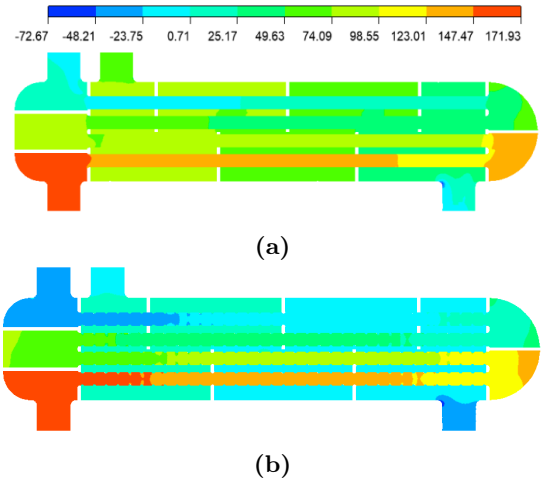

Fig. 11: Pressure (Pa) distribution along y-z section plane at the mid-section of heat exchanger for (a) STHX-with smooth tubes (b) STHX-with dimpled tubes.

in both cases. Negative pressure is observed at the outlet of the shell-side and tube -side, which is as a result of flow reversal.

3.6. Velocity contour

Figure 12 depicts the plot of average velocity along the axial locations of the shell-side and tube-side for both conventional and dimpled STHEs. Continuous fluctuation of the velocity is encountered in the shell-side as compared to the tube-side, but the velocity in the tube-sides is relatively higher than that of the shell side in

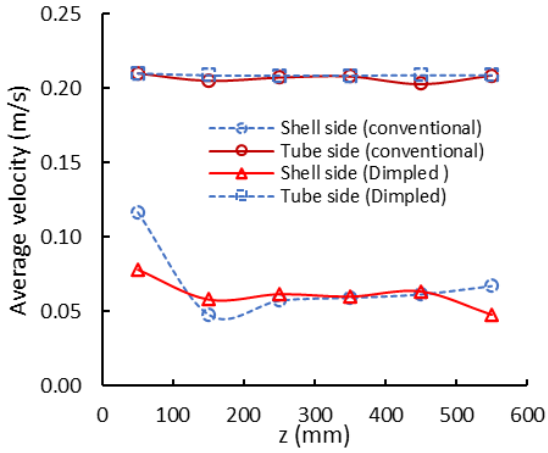

Fig. 12: Average velocity vs z (axial location) for the shell and tube-side of the conventional and dimpled STHEs.

both cases. This is as a result of the obsruction impeded on the flow by the baffles in the shell. Meanwhile, the higher velocity magnitude is observed in the tube-side of the dimpled STHE than in the tube-side of the conventional STHE. This is due to the reduction in the flow area by the dimples in the tube. Figure 13 presents the velocity distribution along the x-y plane at various axial locations (z-axis), and Fig. 14 visualizes the velocity vector along the y-z plane at the mid-section of the heat exchanger. As revealed in Fig. 13 and Fig. 14, the intensity of the velocity decreases from the center of the tubes towards the wall.

4. Conclusions

A Commercial CFD program, ANSYS (Fluent) is used to perform a 3D numerical analysis for STHE with dimpled tubes and conventional STHE (smooth tubes). The thermal and flow characteristics of conventional STHE was compared with that of dimpled tubes STHE. However, the results show that the overall heat transfer coefficient is improved by 14.2%, temperature change at the tube side increased by 15%, and pressure drop is increased by 22% in a shell-and-tube heat exchanger with dimpled tubes as compared to conventional STHE.

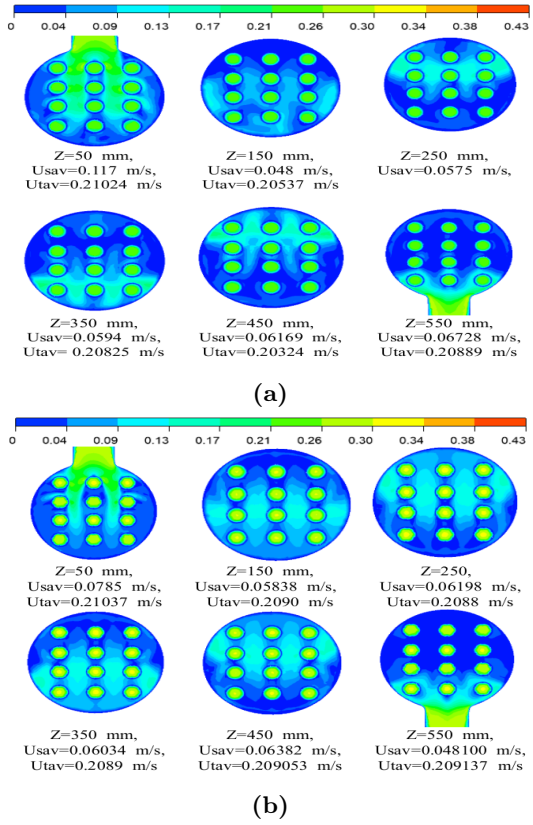

Fig. 13: (a) Velocity (m/s) contour plot along x-y section plane at various axial locations (z-axis) in both shell side and tube side for STHX with smooth tubes. (b) Velocity (m/s) contour plot along x-y section plane at various axial locations (z-axis) in both shell side and tube side for STHE with dimpled tubes.

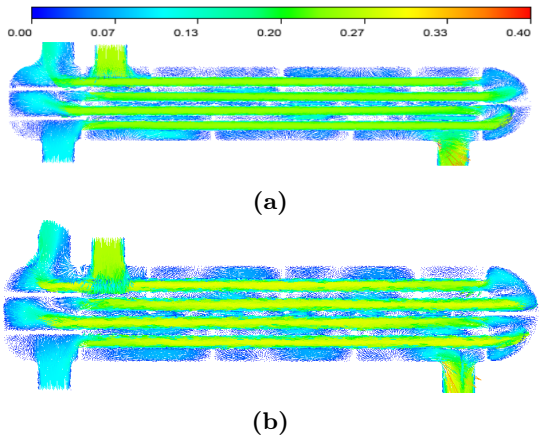

Fig. 14: Velocity (m/s) vector plot along y-z section plane at the mid-section of the STHE for (a) STHE with smooth tubes (b) STHE with dimpled tubes.

Acknowledgment

The authors appreciate the University of Lagos for their support.

References

[1] Mousa, M.H., Yang, C.M., Nawaz, K., & Miljkovic, N. (2021). Review of heat transfer enhancement techniques in two-phase flows for highly efficient and sustainable cooling. *Renewable and Sustainable Energy Reviews*, 111896.

[2] Almasri, R.A. & Narayan, S. (2021). A recent review of energy efficiency and renewable energy in the Gulf Cooperation Council (GCC) region. *International Journal of Green Energy*, *18*(14), 1441–1468.

[3] Giannetti, N., Milazzo, A., & Saito, K. (2022). Thermodynamic investigation of asynchronous inverse air cycle integrated with compressed-air energy storage. *Journal of Energy Storage*, *45*, 103750.

[4] Pugsley, A., Zacharopoulos, A., & Chemisana, D. (2022). Polygeneration systems in buildings. In *Polygeneration Systems*, Elsevier, 351–410.

[5] Derby, M.M., Adams, A.N., Chakraborty, P.P., Haque, M.R., Huber, R.A., Morrow, J.A., Riley, G.A., Ross, M., Stallbaumer, E.M., Betz, A.R. *et al.* (2020). Heat and Mass Transfer in the Food, Energy, and Water Nexus—A Review. *Journal of Heat Transfer*, *142*(9).

[6] Wang, B., Klemeš, J.J., Li, N., Zeng, M., Varbanov, P.S., & Liang, Y. (2021). Heat exchanger network retrofit with heat exchanger and material type selection: A review and a novel method. *Renewable and Sustainable Energy Reviews*, *138*, 110479.

[7] Qin, N. & Tian, H. (2022). Operational analysis of a newly untreated sewage source heat pump with a plate heat exchanger. *Heat and Mass Transfer*, *58*(4), 683–693.

[8] Goff, H.D. (2019). Dairy product processing equipment. In *Handbook of Farm, Dairy and Food Machinery Engineering*, Elsevier, 245–265.

[9] Chandrasekaran, R., Xuejun, Q., Seong, L. *et al.* (2021). Thermal performance evaluation and analysis of the efficient and sustainability shell and tube heat exchanger system. *Journal of Construction Project Management and Innovation*, *11*(1), 151–159.

[10] Qian, X., Yang, Y., & Lee, S.W. (2020). Design and evaluation of the lab-scale shell and tube heat exchanger (STHE) for poultry litter to energy production. *Processes*, *8*(5), 500.

[11] Soltani, H., Soltani, M., Karimi, H., & Nathwani, J. (2022). Optimization of shell and tube thermal energy storage unit based on the effects of adding fins, nanoparticles and rotational mechanism. *Journal of Cleaner Production*, *331*, 129922.

[12] Albdoor, A., Ma, Z., Al-Ghazzawi, F., & Arıcı, M. (2022). Study on recent progress and advances in air-to-air membrane enthalpy exchangers: Materials selection, performance improvement, design optimisation and effects of operating conditions. *Renewable and Sustainable Energy Reviews*, *156*, 111941.

[13] Malika, M., Bhad, R., & Sonawane, S.S. (2021). ANSYS simulation study of a low volume fraction CuO–ZnO/water hybrid nanofluid in a shell and tube heat exchanger. *Journal of the Indian Chemical Society*, *98*(11), 100200.

[14] Hajabdollahi, H., Ataeizadeh, M., Masoumpour, B., & Dehaj, M.S. (2021). Comparison of the Effect of Various Nanoparticle Shapes on Optimal Design of Plate Heat Exchanger. *Heat Transfer Research*, *52*(3).

[15] Biçer, N., Engin, T., Yaşar, H., Büyükkaya, E., Aydın, A., & Topuz, A. (2020). Design optimization of a shell-and-tube heat exchanger with novel three-zonal baffle by using CFD and taguchi method. *International Journal of Thermal Sciences*, *155*, 106417.

[16] Vignesh, S., Moorthy, V.S., & Nallakumarasamy, G. (2017). Experimental and CFD analysis of concentric dimple tube heat exchanger. *Int J Emerg Technol Eng Res(IJETER)*, *5*(7), 18–26.

[17] Serrao, P., Pawase, H., Prakash, A., & Pandita, V. (2017). Comparison of Overall Heat Transfer Coefficient in Plain and Corrugated Pipe and It's CFD Analysis. *International Journal of Advances in Engineering & Technology*, *10*(4), 523.

[18] Xie, S., Liang, Z., Zhang, L., & Wang, Y. (2018). A numerical study on heat transfer enhancement and flow structure in enhanced tube with cross ellipsoidal dimples. *International Journal of heat and mass transfer*, *125*, 434–444.

[19] Banekar, Y.D., Bhegade, S.R., & Sandbhor, M.V. (2015). Dimple tube heat exchanger. *International Journal of Science, Engineering and Technology Research*, *4*(5), 1632–1635.

[20] Matos, R., Vargas, J., Laursen, T., & Saboya, F. (2001). Optimization study and heat transfer comparison of staggered circular and elliptic tubes in forced convection. *International journal of heat and mass transfer*, *44*(20), 3953–3961.

[21] Jozaei, A., Ghafouri, A., & Navaei, M. (2015). Effect of Number of baffles on pressure drop and heat transfer in a shell and tube heat exchanger. *WASET Intl J Mech Aero Indus Mecha and Manuf Eng*, *2*(1), 18303–18312.

[22] Li, Z., Davidson, J.H., & Mantell, S.C. (2006). Numerical simulation of flow field and heat transfer of streamlined cylinders in cross flow. *Journal of heat transfer*, *128*(6), 564–570.

[23] Shahdad, I. & Fazelpour, F. (2018). Numerical analysis of the surface and geometry of plate fin heat exchangers for increasing heat transfer rate. *International Journal of Energy and Environmental Engineering*, *9*(2), 155–167.

[24] Sridharan, M. (2020). Application of fuzzy logic expert system in predicting cold and hot fluid outlet temperature of counter-flow double-pipe heat exchanger. In *Advanced Analytic and Control Techniques for Thermal Systems with Heat Exchangers*, Elsevier, 307–323.

[25] Bari, S. & Hossain, S.N. (2013). Waste heat recovery from a diesel engine using shell and tube heat exchanger. *Applied Thermal Engineering*, *61*(2), 355–363.

[26] Mohanty, S. & Arora, R. (2020). CFD Analysis of a Shell and Tube Heat Exchanger with Single Segmental Baffles. *International Journal of Automotive and Mechanical Engineering*, *17*(2), 7890–7901.

[27] Ozden, E. & Tari, I. (2010). Shell side CFD analysis of a small shell-and-tube heat exchanger. *Energy Conversion and Management*, *51*(5), 1004–1014.

[28] Wang, G., Wang, D., Peng, X., Han, L., Xiang, S., & Ma, F. (2019). Experimental and numerical study on heat transfer and flow characteristics in the shell side of helically coiled trilobal tube heat exchanger. *Applied Thermal Engineering*, *149*, 772–787.

[29] Zhang, J.F., He, Y.L., & Tao, W.Q. (2009). 3D numerical simulation on shell-and-tube heat exchangers with middle-overlapped helical baffles and continuous baffles–Part I: Numerical model and results of whole heat exchanger with middle-overlapped helical baffles. *International Journal of Heat and Mass Transfer*, *52*(23-24), 5371–5380.

[30] Tiwari, A.K., Ghosh, P., & Sarkar, J. (2015). Particle concentration levels of various nanofluids in plate heat exchanger for best performance. *International Journal of Heat and Mass Transfer*, *89*, 1110–1118.

[31] Movassag, S.Z., Taher, F.N., Razmi, K., & Azar, R.T. (2013). Tube bundle replacement for segmental and helical shell and tube heat exchangers: Performance comparison and fouling investigation on the shell side. *Applied Thermal Engineering*, *51*(1-2), 1162–1169.

[32] El Maakoul, A., Laknizi, A., Saadeddine, S., El Metoui, M., Zaite, A., Meziane, M., & Abdellah, A.B. (2016). Numerical comparison of shell-side performance for shell and tube heat exchangers with trefoil-hole, helical and segmental baffles. *Applied Thermal Engineering*, *109*, 175–185.

[33] Wang, Y., He, Y.L., Lei, Y.G., & Zhang, J. (2010). Heat transfer and hydrodynamics analysis of a novel dimpled tube. *Experimental thermal and fluid science*, *34*(8), 1273–1281.

About Authors

Ibrahim Ademola FETUGA is a research scholar at University of Lagos. He had a National Diploma in Marine Engineering at Federal College of Fisheries and Marine Technology, Nigeria. He obtained his B.Eng. in Petroleum Engineering from University of Benin, MSc in Occupational Health and Safety Management from South America University, Delware, MSc in Mechanical Engineering from University of Lagos, and Post-graduate National Diploma in Petroleum Geoscience from Laser Centre of Petroleum Geoscience, Nigeria. His research interests include Computation Fluid Dynamics, nanotechnology, turbo machinery, biomechanics, sustainable and green energy.

Olabode OLAKOYEJO has expertise in computational heat transfer/fluid flow with application of heat generating equipment at Macro, Micro and Nano-scale levels using constructal theory, design and optimization which are critical to the modern technology and development. Also, he is into renewable energy such as biomass and solar due to the challenge of the electricity problem in Nigeria despite the abundant of sun in Africa particularly Nigeria. He is currently working as a Senior Lecturer at University of Lagos, where he teaches, researches and practices Mechanical Engineering. Also, he is Principal Investigator of Royal Society Research Laboratory, University of Lagos. He got his Ph.D. degree in Mechanical Engineering at University of Pretoria, South Africa, He was once a visiting Scholar (Spring, 2016) on MIT-Empowering the Teachers (MIT-ETT) fellowship, Massachusetts Institute of Technology (MIT), United States of America. He has attended and presented at different international conference. He is a member of different professional bodies, including: American Society of Mechanical Engineers (ASME), South African Institution of Mechanical Engineers, Nigerian Institution of Mechanical Engineers, Council for the Regulation of Engineering in Nigeria (Registered Engineer, COREN) and Nigerian Society of Engineers.

Adeola S. SHOTE holds B.Sc. (2005) and MSc (2010) degrees in Mechanical Engineering from Obafemi Awolowo University, Ile-Ife, Nigeria. He later obtained his PhD from the Department of Mechanical and Aeronautical Engineering, University of Pretoria, South Africa. His research area centers on turbine aerodynamics and heat transfer, heat augmentation in channels. He is well grounded in CFD modeling and analysis. He is a member of (1) American Society of Thermal and Fluids Engineers (ASTFE); (2) Aeronautical Society of South Africa (AESSA) and (3) Council for the Regulation of Engineering in Nigeria (COREN).

Gbeminiyi SOBAMOWO obtained OND and H.N.D form The Polytechnic, Ibadan in 1998 and 2002, respectively. He also obtained B.Sc., M.Sc. and Ph.D. in 2006, 2009 and 2013, respectively in the Department of Mechanical Engineering, University of Lagos, Nigeria. He currently a Senior Lecturer in the Department of Mechanical Engineering, University of Lagos. Sobamowo has published over 250 research papers in various prestigious international journals. He is the author of the textbook "Student's Companion for Excellent Performance in Final Year Project and also a co-author of a Textbook on Fluid Mechanics and Hydraulic Machines. Sobamowo is a reviewer for many international and local journals. He is a co-editor of various international journals. He is the founder and principal researcher of Herzer Modelling and Simulation Research Group and also, Renewable Energy-For-Cold Chain

Research Group, Energy System Modeling and Simulations, University of Lagos, Nigeria. He is an inventor of the software "GEM" (General Empirical Modeler). His research interests include energy systems modelling, simulation and design, renewable energy systems analysis and design, flow and heat transfer and thermal fluidic-induced vibration in energy systems. He has supervised and still supervising B. Sc., M.Sc. and Ph.D. students on these research areas. He is a member of the Nigerian Institution of Mechanical Engineers, Nigeria Society of Engineers, and the Council of Regulation of Engineering in Nigeria. His areas of specialization include Energy Systems Modelling, Simulations and Design.

Omotayo OLUWATUSIN is a Lecturer in the Department of Mechanical Engineering at the University of Lagos, his specialization is Biomechanics and thermofluid Engineering, he attended the University of Lagos between 1977 to 1981 for his Bachelor's degree, 1983 to 1985 for his M.sc degree. He also obtained his Ph.D. from University of Lagos; he has 17 years' experience in the Nigerian Hydrocarbon Industry prior to his 18 years teaching and research experience at Lagos State Polytechnic for 2 years and the University of Lagos for 16 years.

Joshua GBEGUDU is a Research scholar at University of Lagos, He obtained his B.Eng. in Petroleum Engineering from the University of Benin in 2014, and his M.sc in Mechanical Engineering in 2020 from University of Lagos. His research interests are nanofluid, renewable energy, computational fluid dynamics, data mining, big data engineering, cloud computing and machine learning.